JOURNAL OF MATERIALS SCIENCE 32 (1997) 5697–5702

NMR characterization of silicon nitride: slurry homogeneity by T_2-weighted proton imaging

PU SEN WANG
Ceramics Division, Materials Science and Engineering Laboratory, National Institute of Standards and Technology, Gaithersburg, MD 20899 USA

The Si_3N_4/water slurries were studied by proton nuclear magnetic resonance (^1H NMR) imaging for homogeneity. ^1H nuclear spin echo signals from Si_3N_4/water slurries were observed by a $(\pi/2)$–τ–π–τ-echo pulse sequence. Bloch's equations were used to calculate the spin–spin relaxation times (T_2) from these echo intensities. The T_2 for the protons in these slurries was measured to be 53.7 ± 0.1 ms. The T_2-weighted imaging technique utilizing $(\pi/2)$–τ–π–τ multiple pulse sequence was mixed with a "shape pulse" for radio frequency (RF)-excitation to detect nuclear spin echo signals for image construction. Sinc shape pulses were used to mix with both the $(\pi/2)$ and the π pulses as a frequency carrier because of the mobility of water molecules in the slurry. The nuclear spin echo intensities were transformed into three-dimensional pictures by magnetic field gradients generated by coils along *x*, *y* and *z*-co-ordinates. Axial-section slices were taken to map the water distribution of the slurry in an NMR tube. A stable and well-dispersed Si_3N_4/H_2O slurry, with ammonium polymethacrylate as dispersant, was observed for several hours. Agglomerization of this slurry was detected after 15 h of standing and NMR imaging shown in contour plots depicted clearly the location and the degree of agglomerization. The water distribution can also be presented in three dimensions by stack plotting of the water intensity profiles.

1. Introduction

A homogeneous slurry is a prerequisite for a homogeneous green body. Surfactants are often added to a slurry as dispersants to improve homogeneity. However, most ceramic powders contain a layer of native surface oxide and possibly other chemical impurities because of exposure to the processing environment. The surface properties of the powders may be different because of different processing parameters. The slurries formed by mixing these powders with polymeric surfactants in an aqueous or non-aqueous environment thus may have different properties even though the composition is nominally the same. This variation can result in a poor reproducibility of ceramic components.

The dispersants in a slurry are necessary to prevent powder agglomeration due to the interaction of the particles through their steric or electrosteric forces. Polyacrylates are one of the most commonly used dispersants for the slurries of oxide or non-oxide ceramic powders where stabilization of particles is maintained by electrostatic adsorption of a polyacrylic ion on the negatively charged particle. The interfacial interactions among powder surface, water, impurities and organic surfactants are very complex and yet not well understood. These interactions result in the formation of inhomogeneous suspensions and thus poor density distribution in green bodies. The resulting agglomerates, inhomogeneous distribution of surfactants, voids and chemical segregation are often the original causes of the defects that cause ceramic components to fail. These defects are considered to be the main cause of problems associated with the repeatability of manufacturing processes. Techniques for the characterization of slurries and green compacts are thus necessary to enhance quality control.

Nuclear magnetic resonance (NMR) imaging is a non-destructive technique which can provide a unique material diagnostic mapping. It may provide information on both material distribution (nuclear spin density) and chemistry if the monitoring nuclei have differentiable spin relaxation times. The imaging method uses a magnetic field gradient to encode the positions of the nuclear spins with a spatially varying Larmor frequency. Once the variations in resonant frequency have been decoded, an image of NMR parameters can be created. Several studies have been published in the literature for NMR imaging application in ceramics [1–11]. Most of these studies involve green bodies and binder distributions. We have previously published such a study to investigate the silicon nitride binder distribution by monitoring proton-containing binders. Because of the sample location in that study utilized the stray field as gradient, protons resonated at 163 MHz, instead of 400 MHz, as would have been the case in a field gradient generated by coils. However, the field gradient provided by such a stray-field on a specific planar surface in

0022–2461

a 9.394 T superconducting magnet is much larger than that being generated by the coils [1]. We have also published the results, in two parts, of NMR spin–spin relaxation study and spin–spin relaxation time (T_2) weighted ^{1}H imaging on injection-moulded alumina green compacts [2, 3]. In the first part of these two papers, proton NMR analysis near 400 MHz (400.159972 MHz) was developed to evaluate the binder in green injection-moulded alumina compacts [2]. The T_2 of protons in the binder components (paraffin wax, polypropylene and stearic acid) were measured to allow comparison with those in the injection-moulded green compacts. ^{1}H nuclear spin echo signals were observed by a $(\pi/2)$–τ–π–τ-echo pulse sequence and Bloch's equations were used to calculate the spin–spin relaxation times from these echo intensities. Binder content variations in three green compacts moulded from the same nominal blend composition were detected. Analysis of the moulded compacts also showed the presence of a specie with a T_2 value near 300 μs. This species may be the result of reaction during processing or the presence of moisture.

The second part involves the study of the binder distribution of these green compacts by proton NMR imaging [3]. The solid imaging technique of T_2-weighted imaging at 400.159972 MHz was used for this study. The imaging technique utilizes a multiple pulse sequence for echo detection and phase encoding. Two- and three-dimensional images were constructed from the intensities of these nuclear echo signals. The spatially resolved two-dimensional images obtained by application of this technique indicated that the green compacts fabricated from the same nominal binder composition did not have the same content as expected. This observation agreed well with our previous conclusion drawn from nuclear spin echo studies by Hahn's pulse sequence. A $64 \times 64 \times 64$ three-dimensional imaging revealed that binder distribution inhomogeneity and internal imperfections do exist in certain parts of the samples. A binder-rich folding line was also detected in one of these green compacts.

In the present paper, water proton spin densities in Si_3N_4/H_2O slurries are used to construct NMR images for monitoring slurry homogeneity.

2. Experimental procedure*

2.1. Silicon nitride slurry

Ube SN-E-10 silicon nitride was added to distilled water and the slurry was adjusted with 12.5 g l^{-1} (0.5 M) NH_4OH to a pH of 9.0. This slurry contained 20% Si_3N_4 in mass fraction and 350 p.p.m. ammonium polymethacrylate (Darvan C™ by R. T. Vanderbilt) as a dispersant. The Si_3N_4 powder had a median particle size of 0.2 μm and specific surface area of 10 m^2 g^{-1}. The slurry was subjected to ultrasonic vibration at 40 W for 1 min and allowed to stand for 1 min. This procedure was repeated three times for the slurry. The slurry was then transferred to a 10 mm diameter, thin wall, NMR tube for measurement. The inner diameter of this tube was 9.07 $\pm$ 0.01 mm ($\pm$ 1 standard deviation).

2.2. NMR micro-imaging facility

The NMR imaging facility consists of a Bruker MSL-400 system with micro-imaging accessories. This spectrometer has a superconducting magnet of 9.394 T which corresponds to ^{1}H resonant frequency of $\sim$ 400 MHz. Our actual resonant frequency was 400.140000 $\pm$ 0.000001 MHz. A 10 mm RF-coil was used for detecting nuclear spin–echo signals of the water protons in the slurry. A $(\pi/2)$–τ–π–τ-echo pulse sequence was used for echo detection. In this sequence, τ is a delay for nuclear dephasing on xy-plane and $\pi/2$ is a 90° RF-pulse to flip the nuclear magnetization moment, M, from the z-axis to the y-axis. During the τ period, the components of M_{xy}, the xy-component of M, dephased because of their characteristic T_2. A π (180°) pulse was then applied to the sample to farther rotate the dephased M_{xy} components about the x-axis. An echo signal was recorded after a τ delay from the π pulse. This pulse sequence is a Hahn's sequence [12] and is very similar to the Carr–Purcell/Gill–Meiboom sequence [13]. The $\pi/2$ and π pulse width were 7.25 μs and 14.5 μs, respectively.

Since the T_2 is long in slurry, these "hard pulses" were mixed with a "shape pulse" (or "soft pulse") for detection of echoes in a frequency selective manner to select the slice number along the z-axis. This is an important feature of selective excitation of a liquid sample where a large volume of sample may be excited by a RF-pulse. A sinc shape, $[(\sin x)/x]$, was utilized to mix with the hard pulses in this study. The pre-emphasis unit was also adjusted to counter the distortion of the pulse shape due to eddy currents when the gradient coils were switched on.

A set of gradient coils was inserted around the RF-coil to generate a maximum field gradient of approximately 6×10^{-3} T cm^{-1} for phase encoding. The field gradients were driven by two audio power amplifiers from a selective excitation unit (using only three channels out of four). In the multislice technique used in the slurry characterization, an xy mapping indicated that the x-coil was the reading axis and a maximum of 512 points were recorded, the y-coil was the phase-encoding co-ordinate, and the z-co-ordinate was the axis of slicing. The pulse sequence of this multislice technique is shown in Fig. 1. Note that D_{14} was used for both $\pi/2$ and π pulses because they are mixed with the soft pulses. This is contrary to the solid technique where only hard pulse would be used because of short T_2 [3].

*Certain commercial equipment, instruments, or materials are identified in this paper in order to specify adequately the experimental procedure. Such identification does not imply recommendation or endorsement by the National Institute of Standards and Technology, nor does it imply that the materials or equipment identified are necessarily the best available for the purpose.

3. Results and discussion

The nuclear spin–spin relaxation time (T_2) was measured by a multiple pulse sequence of $(\pi/2)_x$–τ–$(\pi)_y$–τ-echo to detect the nuclear echo signals. In this manner, the $(\pi/2)_x$ is a 90° RF-pulse (7.25 μs pulse-width) parallel to the x-axis that flips the nuclear bulk magnetization vector, M, from the z-axis to the y-axis. During the variable delay, τ, the xy-component of this bulk nuclear magnetization vector, M_{xy}, starts to fan out and lose phase coherence on the xy-plane because of the magnetic field inhomogeneity. The $(\pi)_y$ is a 180° pulse (14.5 μs pulse-width) parallel to the y-axis that rotates the dephased M_{xy} components on the xy-plane about the x-axis. A nuclear echo signal is detected at the end of the second delay, τ. Nuclear echo signal intensities were measured for the delays (τ) of 40, 50, 60, 70, 80, 90, 100, 110, 120 and 130 ms in the $(\pi/2)_x$–τ–$(\pi)_y$–τ-echo-D_0 sequence where D_0, a delay of 30 s, is to provide a time for the nuclei to recover their equilibrium between each of the 64 sequences accumulated to get a good signal-to-noise. Fig. 2 shows the echo signals for such a set of τ values from the proton in a Si_3N_4/water slurry. Note that the sweep-widths of these nuclear echo signals are 4310 ± 1 Hz. The echo intensities detected at these delays are also tabulated in Table I for this slurry. The intensities are in an arbitrary units and were measured for the maximum scale in the y-axis of the monitor at $\tau = 40$ ms. A plot of these intensities versus delay times is shown in Fig. 3. This figure shows clearly that the spin echo intensity decays exponentially and approaches 0 when τ is near 130 ms.

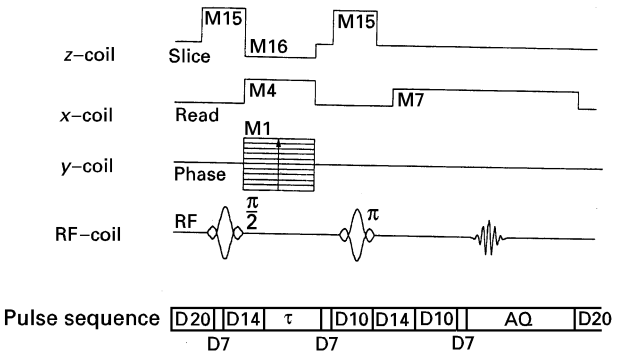

Figure 1 Pulse sequences in the gradient coils and RF-coil during acquisition of a multiple xy-slice NMR image.

According to Bloch's equation

$$dM_x/dt = \gamma(MH)_x - M_x/T_2 \quad (1)$$

and

$$dM_y/dt = \gamma(MH)_y - M_y/T_2 \quad (2)$$

where H is the total magnetic field and γ is the gyromagnetic ratio. The component of the nuclear magnetization vector on the xy-plane will decay

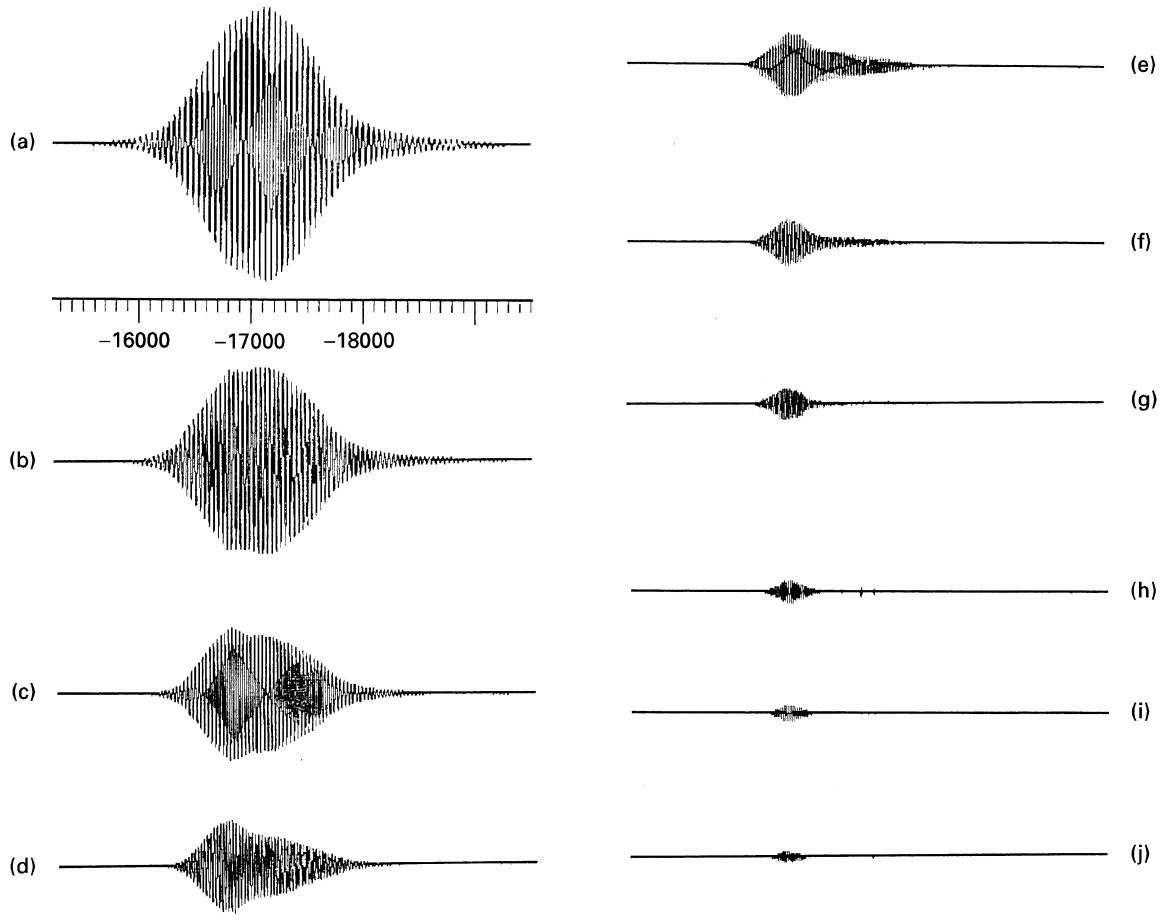

Figure 2 Nuclear spin echo signals from a Si_3N_4/H_2O slurry at τ equals (a) 40, (b) 50, (c) 60, (d) 70, (e) 80, (f) 90, (g) 100, (h) 110, (i) 120, and (j) 130 ms. The unit of the scale is Hz showing a sweep width of 4310 Hz.

TABLE I ^{1}H Spin–echo intensity decay of proton in a Si_3N_4/water slurry

Delay, τ (ms)	Nuclear spin–echo intensity (arbitrary unit ± 1)
40	46
50	32
60	20
70	15
80	11
90	8
100	5
110	4
120	2
130	1

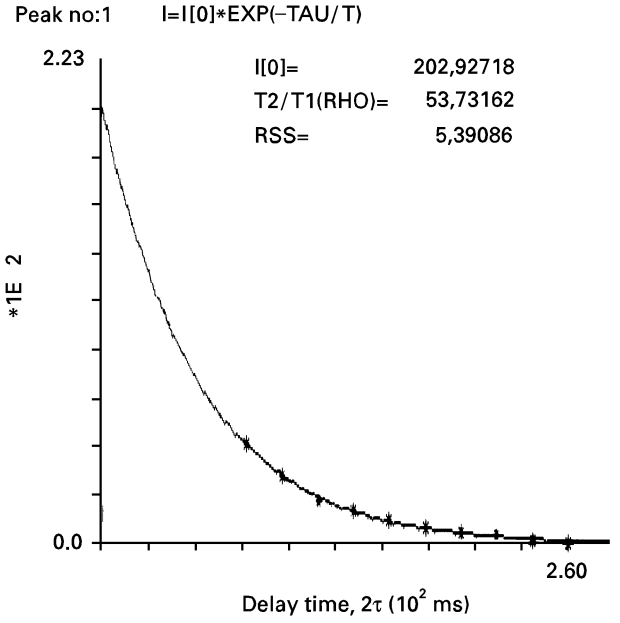

Figure 3 A plot of nuclear spin echo intensities versus various delays (τ) from the data shown in Table I and Fig. 2. An exponential decay can be observed clearly.

exponentially via T_2 causing the spin echo intensity observed at time, t, to exponentially decrease according to

$$I = I_0 \exp(-t/T_2) \quad (3)$$

where I_0 is the echo intensity at equilibrium. T_2 can be calculated by Equation 3 from the values of I and τ when the echo occurs at $t = 2\tau$. T_2 value of 53.7 ± 0.1 ms was obtained by substituting τ and echo intensity values (Table I) into Equation 3.

As mentioned previously, Fig. 1 shows the pulse sequences occurred in the gradient-coils and RF-coil during acquisition of a multiple xy-slice NMR image for a slurry sample. The composite pulse sequence given by the NMR spectrometer is D_{20}–D_7–D_{14}–τ–D_7–D_{10}–$D_{14} - D_{10} - D_7$–AQ–D_{20} and is shown in the bottom of this figure. In the acquisition of such an image, the z-axis is the co-ordinate where multiple slicing will occur and the xy-plane is the one to show water distribution. When acquisition starts, a delay, D_{20}, is required for the synthesizer to generate the frequencies in the computer list. A pulse of D_7 was applied to turn on the z-gradient for slice selection. Then, a $(\pi/2)_x$ RF-pulse was irradiated on the sample from the transmitter to turn the nuclear magnetization vector, M, from the z-axis to the y-axis. However, because the sample is in liquid phase and nuclear spin–crystal lattice relaxation time (T_1) is short, a large portion of the sample will be excited by the RF-pulse. This is not desirable. Consequently, a frequency-selected shape pulse was generated by the selective excitation unit to mix with the RF-pulse in order to localize the excitation. Because of the mixing of the RF-pulse with this soft pulse, D_{14} becomes very long (2000 μs in our experiment as compared to 7.25 μs of π/2 pulse-width). At the end of this mixed pulse, a variable delay, τ, is applied. During this period, the xy-components of the magnetization vector, M_{xy}, are dephasing because of spin–spin interaction. Meantime, all x- and y-gradient coils are turned on for reading and phase encoding, respectively, while the z-coil will be turned off. At the end of τ, all gradient coils are turned off and a period of D_7 is applied for stabilization and D_{10} for T_2-weighting. Then z-coil was turned on once again for slice selection. The same T_2-weighting period of D_{10} is required for the detection of echo signal after a D_{14} of π_x mixed with shape pulse is applied to rotate the dephased M_{xy} components from the $+y$ to the $-y$ axis. The receiver was turned on for a period of AQ for detection of the nuclear echo signal. A negative echo signal was recorded, that is, the echo occurred at the negative y-axis. Finally, a D_{20} lets the excited nuclei release their energy through spin–lattice relaxation and become ready for a new cycle starting with a $(\pi/2)_{-x}$ excitation for recording of a positive echo signal. Fourier transformation of this echo will result in an echo profile of the sample. An example of this profile is given in Fig. 4 from the water in the silicon nitride/water slurry. Note that from one end to the other end of this profile is 9.07 mm, the inner diameter of a 10 mm diameter NMR sample tube. Once this second cycle is finished, the strength of phase encoding in the y-coil was stepped up incrementally for construction of images.

Fig. 5 represents a 1-mm slice of T_2-weighted proton NMR image from a Si_3N_4/H_2O slurry. This sample contains mass fraction of 20% powder, 350 p.p.m. Darvan C™ as dispersant. Profiles can be drawn on the picture along the x-(row) or y-axis (column) to measure water content quantitatively. The top picture shows a profile of uniform water

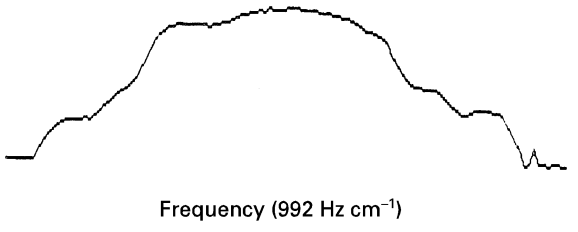

Figure 4 A nuclear spin echo profile of a Si_3N_4/H_2O slurry. Note that the profile width is 9.07 mm which is the inner diameter of a 10 mm NMR tube.

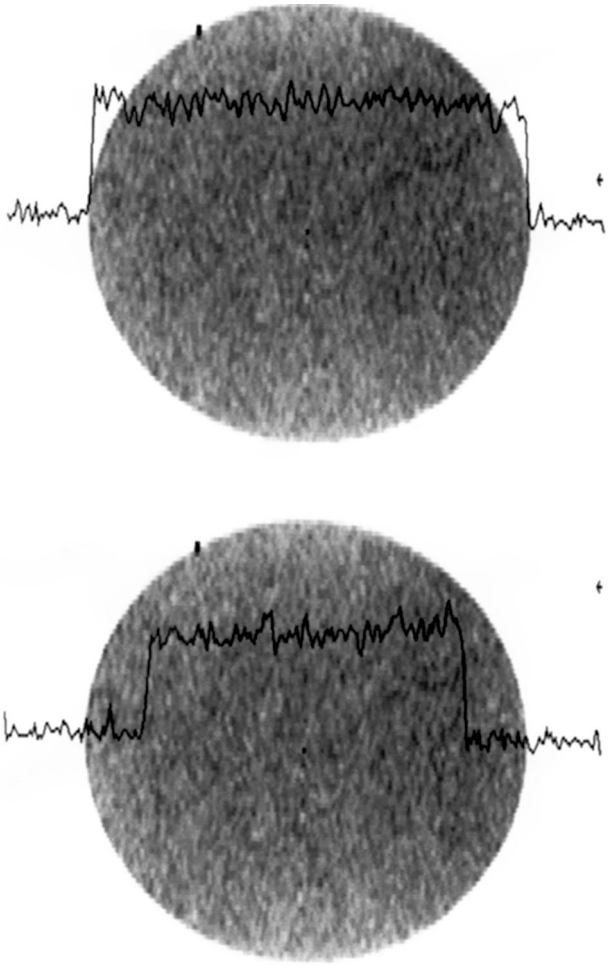

Figure 5 T_2-weighted proton NMR imaging of a Si_3N_4/H_2O slurry. The slice is 1 mm thick. The profiles on this slice show an overall homogeneous water distribution (top); however, at some point, a profile showing slightly higher water content on the right side of the sample was found (bottom). The position of profile is marked by an arrow on the right.

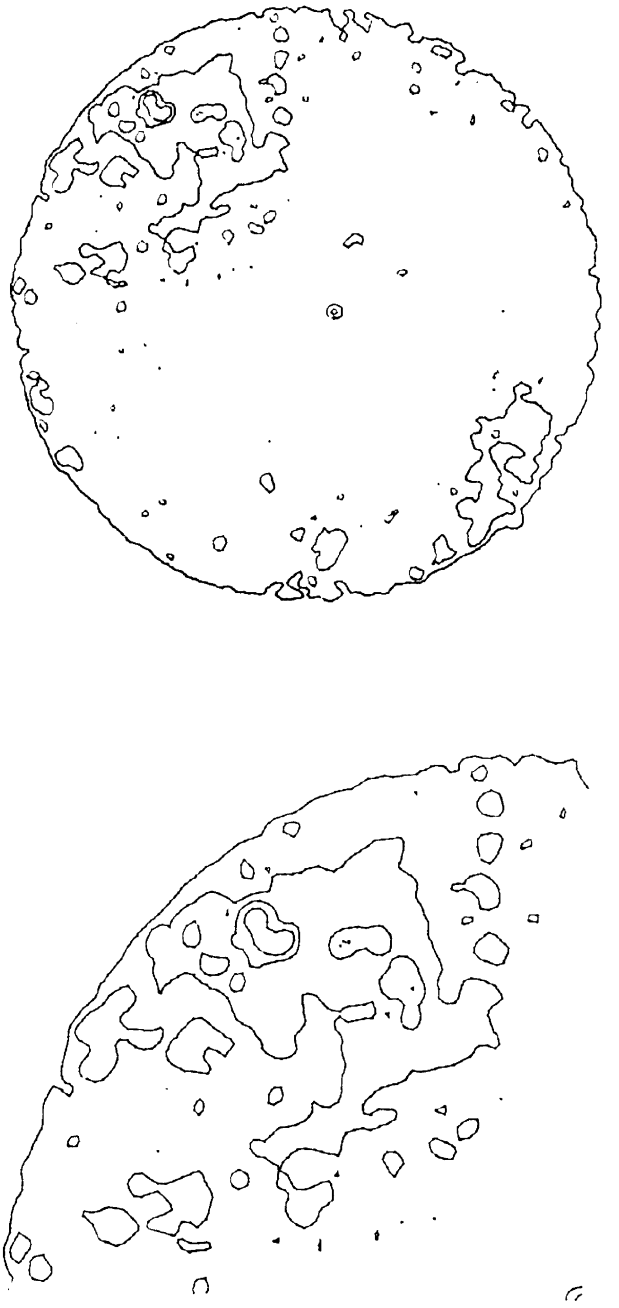

Figure 7 Contour plots of water distribution in the inhomogeneous Si_3N_4/H_2O slurry shown in Fig. 6. The bottom figure is an enlarged high-resolution plot of the left upper quadrant which has a high water content.

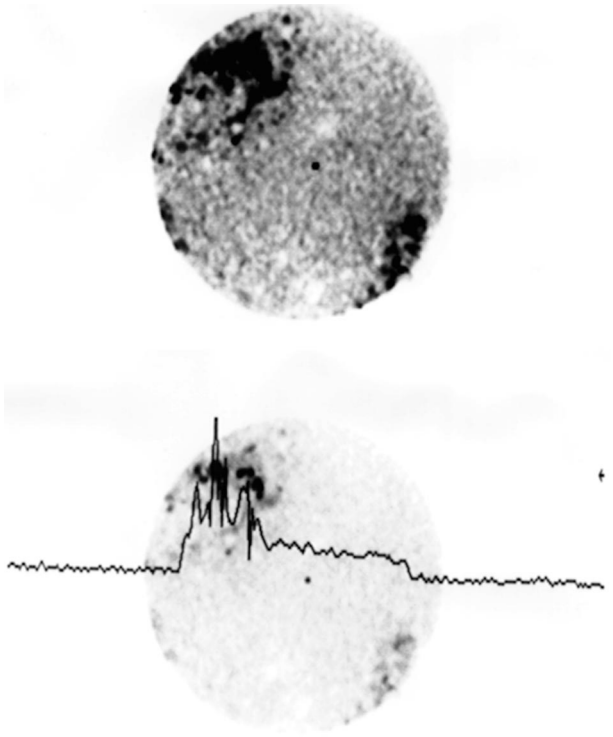

Figure 6 T_2-weighted proton NMR imaging of a Si_3N_4/water slurry 15 h after sample preparation. Powder agglomeration occurred during this period and regions of high water content formed, as can be seen by darker areas this picture. The profile (bottom) on the upper left region of the picture shows at some point water content is five times higher than other region.

distribution along the row indicated by an arrow on the right. Several profiles were examined on this picture and an overall homogeneous slurry was observed. However, at some point, a slightly higher water content on the right side of the sample could be found, as shown in the bottom picture in Fig. 5.

The stability of ceramic powders in a slurry depends on the chemical and physical properties of powders as

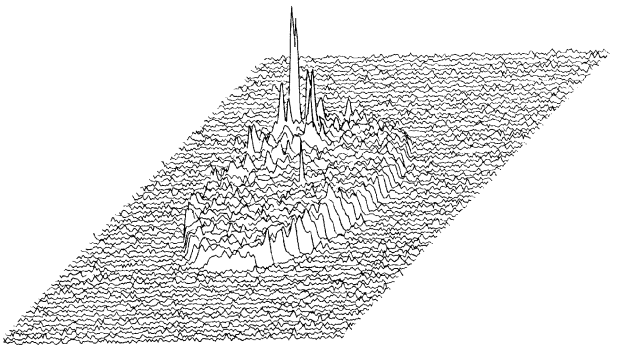

Figure 8 A stack plot of water distribution of the sample shown in Fig. 7. The inhomogeneous water distribution after agglomeration can be presented in three dimensions.

well as the dispersants used. Silicon nitride powders have native surface oxides whose thickness depends on the processing parameters. Darvan C™, which forms polymeric anions in an aqueous solution, appears to interact well with Si_3N_4 powders with thin surface oxide films under our experimental conditions. This interaction force results in a formation of micelle-like molecular groups with Si_3N_4 particles surrounded by polymethacrylate anions. A well-dispersed slurry, such as shown in Fig. 5, will be stabilized for several hours. However, agglomerates will form eventually due to the gravitational force. Fig. 6 is a NMR image of such a slurry 15 h after sonicating. A rather inhomogeneous water distribution was shown in the picture with darker areas representing higher water content. A profile through this picture shows water content is very high in some spots on the upper left quadrant. Note that the spot at the centre is due to baseline noise during echo acquisition.

The contour plots of water distribution of this inhomogeneous Si_3N_4/H_2O slurry are shown in Fig. 7. Each isle represents an area at which the water concentration is different from its neighbours. This contour plot indicates that at the upper left quadrant, the powder agglomeration is most severe and water content is very high. An enlarged high resolution plot is also shown in this figure. Plotting several profiles can provide a methodology to construct a three dimensional picture by stacking the profiles in succession (Fig. 8).

4. Conclusions

Si_3N_4/water slurries were studied by proton NMR imaging for homogeneity. Nuclear spin echo technique and Bloch equations were used to calculate the spin–spin relaxation times. The T_2-weighted imaging technique with "shape pulses" for RF-excitation was used for image construction. A stable and well-dispersed Si_3N_4/H_2O slurry, with ammonium polymethacrylate as dispersant, was observed for several hours.

References

1. P. S. WANG, D. B. MINOR and S. G. MALGHAN, *J. Mater. Sci.* **28** (1993) 4940.
2. P. S. WANG, S. G. MALGHAN, S. J. DAPKUNAS, K. F. HENS and R. RAMAN, *ibid.* **30** (1995) 1059.
3. *Idem.*, *ibid.* **30** (1995) 1069.
4. J. L. ACKERMAN, W. A. ELLINGSON, J. A. KOUTCHER and B. R. ROSEN, "Nondestructive characterization of materials II" (Plenum Press, New York, 1987) p. 129.
5. W. A. ELLINGSON, J. L. ACKERMAN, L. GARRIDO, J. D. WEYAND and R. A. DIMILIA, *Ceram. Engng Sci. Proc.* **8** (1987) 503.
6. J. L. ACKERMAN, L. GARRIDO, W. A. ELLINGSON and J. D. WEYAND, "Nondestructive testing of high-performance ceramics" (American Ceramics Society, Westerville, OH, 1988) p. 88.
7. K. HAYASHI, K. KAWASHIMA, K. ROSE and T. INOUYE, *J. Phys. D*: *Appl. Phys.* **21** (1988) 1037.
8. L. GARRIDO, J. L. ACKERMAN, W. A. ELLINGSON and J. D. WEYAND, *Ceram. Engng Sci. Proc.* **9** (1988) 1465.
9. W. A. ELLINGSON, P. S. WONG, S. L. DIECKMAN, J. P. POLLINGER, H. YEH and M. W. VANNER, *ibid.* **10** (1989) 1022.
10. W. A. ELLINGSON, P. S. WONG, S. L. DIECKMAN, and J. L. ACKERMAN, *Amer. Ceram. Soc. Bull.* **68** (1989) 1180.
11. L. GARRIDO, J. L. ACKERMAN and W. A. ELLINGSON, *J. Magn. Reson.* **88** (1990) 340.

Received 9 September 1996
and accepted 9 May 1997